J Mater Sci (2021) 56:19452–19465

Chemical routes to materials

Dual enhancement of photooxidation and photoreduction activity by coating CdS nanoparticles on lignin-based biomass carbon with irregular flower-like structure

Weilong Shi[1,4], Chunli Shi[2], Wei Sun[2], Yanan Liu[2], Feng Guo[3,*], and Xue Lin[2,*]

[1] School of Material Science and Engineering, Jiangsu University of Science and Technology, Zhenjiang 212003, People's Republic of China
[2] School of Material Science and Engineering, Beihua University, Jilin 132013, People's Republic of China
[3] School of Energy and Power, Jiangsu University of Science and Technology, Zhenjiang, Jiangsu 212003, People's Republic of China
[4] College of Chemistry, Zhengzhou University, Zhengzhou 450001, People's Republic of China

Received: 22 July 2021
Accepted: 4 October 2021
Published online: 12 October 2021

ABSTRACT

Energy crisis and environmental pollution have become two major problems facing mankind. Photocatalytic hydrogen production and degradation of organic pollutants using solar light is a promising solution. Thus, the study of efficient, environmentally friendly and stable photocatalysts has been an important research topic for many researchers over the years. In this study, lignin-based biomass carbon was first used as a carbon source and compounded with CdS nanoparticles to prepare CdS/LC composite. The resulting CdS/LC photocatalyst not only solves the high agglomeration of CdS nanoparticles, but also presents excellent photocatalytic activity and high stability. The optimal CdS/LC-3 exhibits high photocatalytic degradation rate and photocatalytic hydrogen evolution rate, which are about 2.3 and 3.73 times higher than those of pure CdS, respectively. This research work provides a new and effective way for the utilization of lignin, which makes the high-quality utilization of lignin possible.

Handling Editor: Pedro Camargo.

Address correspondence to E-mail: gfeng0105@126.com; jlsdlinxue@126.com

https://doi.org/10.1007/s10853-021-06589-4

Introduction

The serious pollution of the environment and the rapid consumption of fossil fuels are the serious problems facing mankind [1–3]. Thus, human beings must develop sustainable renewable energy to reduce dependence on fossil fuels and pollution emissions. As we known, hydrogen energy is recognized as a clean energy, as a low-carbon and zero-carbon energy is emerging [4–6]. And photocatalytic water splitting for hydrogen production provides a promising method for obtaining the energy needed by human beings [7–9]. Meanwhile, ciprofloxacin (CIP) is a frequently used wide-spectrum antibacterial drug with the characteristics of strong permeability, strong bactericidal ability and fast speed. Because of its widely used and lack of effective treatment processes, it can accelerate bacterial resistance in terms of surface water and cause biological toxicity, which brings huge threats to human health and the safety of the entire ecosystem [10, 11]. Fortunately, photocatalytic technology can also be used effectively to degrade organic pollutants for reducing environmental pollution [12–18]. Therefore, how to construct effective photocatalyst to improve photooxidation and photoreduction activity is the focus of current researchers.

Cadmium sulfide (CdS) has a band gap that is close to the optimum value for solar energy conversion and therefore possesses a high visible light absorption coefficient, which can be used as a promising visible-light-driven photocatalyst [19, 20]. However, under long-term irradiation, its structure will be destroyed due to severe photo-corrosion. In addition, CdS nanoparticles may suffer from a large amount of aggregation, resulting in a decrease in specific surface areas and a scarcity of active sites [21, 22]. For the purpose of solving the problem of aggregation and photo-corrosion of CdS photocatalysts, various corresponding studies have been carried out, such as loading precious noble metals, forming solid solutions and constructing semiconductor heterojunctions [23, 24]. However, these methods require complex preparation processes as well as expensive fabrication costs, and it is of utmost importance to develop a simple and cost-effective method for ameliorating CdS. Recently, immobilization of CdS nanoparticles on the surface of carbon materials with high specific area (such as graphene, carbon nanotube, fullerene, etc.) can effectively solve their agglomeration problems [25].

Compared with traditional carbon materials, biomass carbon is renewable and inexpensive, which is in line with the path of sustainable development [26–29]. Biomass is rich in cellulose, hemicellulose and lignin, among which lignin is a renewable biomass resource with abundant reserves, second only to cellulose, and widely exists in wood, sorghum, corncob and other plant resources [30, 31]. However, in most cases, lignin is considered only as a biomass waste in the pulp industry, and more than 95% of it is thrown into rivers or burned after concentration [32]. In particular, a large amount of industrial lignin from the paper industry and bioengineering is used as an industrial by-product and less than 2% is recycled as a chemical feedstock, which not only wastes resources, but also causes environmental problems [33, 34]. In addition, lignin is an aromatic ring structure containing various functional groups consisting of carbon, hydrogen, oxygen and a small amount of nitrogen with nearly 60% carbon, and these advantages make lignin an ideal choice for biomass carbon [35, 36], which can not only turn waste into treasure, but also improve its high-quality application effectively. Biomass ethanol lignin is a by-product of the fuel production process from maize straw and wheat straw, which is cheap and easy to obtain and has not been treated with high temperature, pressure or acid or alkali, so it is naturally well preserved. Hence, it is a challenge to use biomass ethanol lignin as a biomass carbon source precursor to modify CdS for enhancing its photocatalytic activity, which has not been reported before.

In this study, biomass ethanol lignin was used as a biomass carbon source to modify CdS nanoparticles to form composite photocatalyst for the photocatalytic degradation of ciprofloxacin and hydrogen production performance under visible light irradiation. The photocatalytic enhancement mechanism of photooxidation and photoreduction activity was proposed based on various characterization tests.

Experimental section

Materials

Biomass ethanol lignin was provided from Jilin Fuel Ethanol Co, Ltd. Ciprofloxacin (CIP), cadmium

dihydroacetate ($Cd(CH_3COO)_2•2H_2O$), magnesium oxide (MgO), p-benzoquinone (p-BQ), triethanolamine (TEOA), isopropanol (IPA) were purchased from Macklin's Reagent Co., Ltd. Lactic acid was purchased from Sinopharm Group Chemical Reagent Co., Ltd. Ethanol and dimethyl sulfoxide (DMSO) were from Tianjin Damao Chemical Reagent Factory. Distilled water was supplied by UPT-A (Shanghai Shenfen Analytical Instrument Co., Ltd.). All chemical reagents are analytical purity and can be used without further purification.

Synthesis of lignin carbon (LC)

The mass ratio of lignin to MgO (2:1) was dispersed in 40 mL of distilled water and stirred vigorously for 30 min. Subsequently, the mixed solution was continued at 100 °C to evaporate the water in the mixture. The dried sample was ground and transferred to a tube furnace for calcination at 600 °C with the heating rate of 5 °C min^{-1} under N_2 atmosphere for 2 h. The resulting sample was then added to dilute hydrochloride acid solution (1 mol/L) and stirred for 1 h to remove the template. After thorough washing with pure water, the LC powder was collected.

Synthesis of CdS/LC composites

CdS/LC composites with different mass ratios were prepared and the specific synthetic route is shown in Scheme 1. Firstly, 0.213 g of $Cd(CH_3COO)_2•2H_2O$ and different weights of LC (0.01 g, 0.03 g, 0.05 g and 0.07 g) were added to 80 mL of DMSO. After that, the mixed solution was stirred vigorously for 0.5 h and ultrasonically treated for 0.5 h. Next, the above solution was transferred to a 100 mL autoclave and kept at 180 °C for 12 h. When the temperature dropped to room temperature, it was washed three times with ethanol and finally dried in an oven at 80 °C. The resulting products were abbreviated as CdS/LC-1, CdS/LC-3, CdS/LC-5 and CdS/LC-7, respectively. Pure CdS sample was prepared under the same synthetic conditions without the addition of LC.

Photocatalytic degradation experiment of ciprofloxacin (CIP)

The photocatalytic activity of as-prepared samples was tested in a photochemical protection chamber (CEL-LB70-5, Beijing Zhongjiao Jinyuan Technology Co., Ltd.) by degrading CIP under visible light at room temperature environment. A 500 W Xe lamp with UV cut-off filter ($\lambda > 420$ nm) was used as the visible light source. Firstly, 30 mg of photocatalyst was added to 100 mL of CIP solution (50 mg/L), and then the suspension was magnetically stirred for 30 min to reach adsorption–desorption equilibrium in the dark. During the photocatalytic reaction, 5 mL suspension was extracted after centrifugation and analyzed by UV–visible spectrophotometer at 276 nm to evaluate the photocatalytic activity based on the following equation:

Scheme 1 Schematic route steps of LC and CdS/LC composite photocatalyst.

$$\text{Degradation}\ (\%) = (1 - C/C_0) \times 100\% \quad (1)$$

C_0 represents the absorbance of the initial concentration of CIP solution and C represents the absorbance of the CIP solution concentration after the photo-reaction.

Photocatalytic hydrogen production experiment

For photocatalytic hydrogen production test, 30 mg of photocatalyst was taken and dissolved in 100 mL of solution (90 mL of water and 10 mL of lactic acid as the sacrificial agent). Then, 3 wt.% of Pt was added to the photocatalytic system as a co-catalyst to facilitate the hydrogen evolution reaction. All the above experimental steps were carried out under magnetic stirring. Visible light was provided by a Xenon lamp equipped with a long-pass wavelength of $\lambda > 420$ nm. The temperature of the cooling water in the cooling circulation system was maintained at 5 °C. The on-line GC-7920 gas chromatograph (GC) was set up with a thermal conductivity detector (TCD) and a 5 Å molecular sieve column with N_2 and air as carrier gases for detection.

The detailed characterizations, photoelectrochemical and active species capture tests are provided in Supporting Information.

Results and discussion

The crystal structure of the as-prepared LC, pure CdS and CdS/LC-3 samples was characterized by X-ray diffraction (XRD) and is shown in Fig. S1. As can be seen, the broad characteristic diffraction peaks of LC at about 21.9° and 42.3° can be indexed to the (002) and (100) crystal planes of graphitic carbon (JCPDS NO. 41–1487) [37] Moreover, the XRD pattern of CdS clearly displays that three distinct peaks of pure CdS at 26°, 44° and 52.1° can be indexed to (111), (220) and (311) planes of CdS (JCPDS 80–0019), respectively [38]. The XRD pattern of CdS/LC-3 composite shows similar peaks to those of pure CdS and exhibits a slight fluctuation at 21.9°, indicating CdS particles were successfully loaded on LC surface to form CdS/LC composite [39]. To investigate the functional groups of as-prepared products, Fourier transform infrared (FT-IR) spectra of LC, CdS and CdS/LC-3 were carried out (Fig. S2). The FT-IR spectrum of LC shows that the peak near 3430 cm^{-1} is due to the stretching vibration of the hydroxyl group (•OH) and the peak at 1550–1650 cm^{-1} indicates aromatic skeletal vibrations (C–C/C-O) [40, 41]. The FT-IR spectra of pure CdS and CdS/LC-3 composite exhibit similar peaks, with peaks around 2900–2800 cm^{-1} are attributed to C-H stretching vibrations and Cd–O stretching vibrations, and other peaks at the ranges of 1410–1380 cm^{-1} are ascribed to Cd-S bonds [42]. Moreover, the peaks corresponding to pure CdS in the CdS/LC-3 composite remained unchanged, indicating that the chemical structure of CdS was not changed after loading on the LC. Fig. S3 shows the Raman spectra of as-prepared samples to further confirm the composition of materials. Raman analysis of the pure CdS nanoparticles exhibits that the characteristic Raman peaks at around 290 cm^{-1} and 584 cm^{-1} are assigned to longitudinal optics arising from A1 mode Cd-S bond vibrations [43, 44]. In the Raman spectra of the LC and CdS/LC-3 samples, it can be observed that the two peaks at 1343 and 1597 cm^{-1} are responsible for D-band and G-band, which are due to ring breathing vibrations of the condensed benzene ring in the partially hydrogenated amorphous carbon material and the in-plane bond stretching motion of the sp^2 carbon atom pair in the aromatic and olefin molecules [45]. In addition, a 2D-band at 2892 cm^{-1} can be found in LC indicates a high degree of crystallinity of LC, which is ascribed to the fact that $Mg(OH)_2$ acts as a structural guide to improve the disordered structure of lignin during water evaporation, allowing LC to obtain a high degree of graphitization and crystallinity after carbonization [46]. This improvement facilitates the fast shuttle of electrons so that LC can effectively suppress the fast recombination of electron–hole pairs over CdS.

The surface morphology and elemental distribution of the composite photocatalyst were given through using scanning electron microscope (SEM), transmission electron microscopy (TEM), high-resolution transmission electron microscopy (HRTEM) and elemental mapping techniques (Fig. 1). As displayed in Fig. 1a, the CdS exhibits a spherical morphology with the particle size of 100–200 nm, which are agglomerated together. And the LC sample presents an irregular curl-like structure with abundant holes and channels, which may be due to the caking of the released gas after calcination (Fig. 1b). In Fig. 1c, it can be seen that a large number of CdS

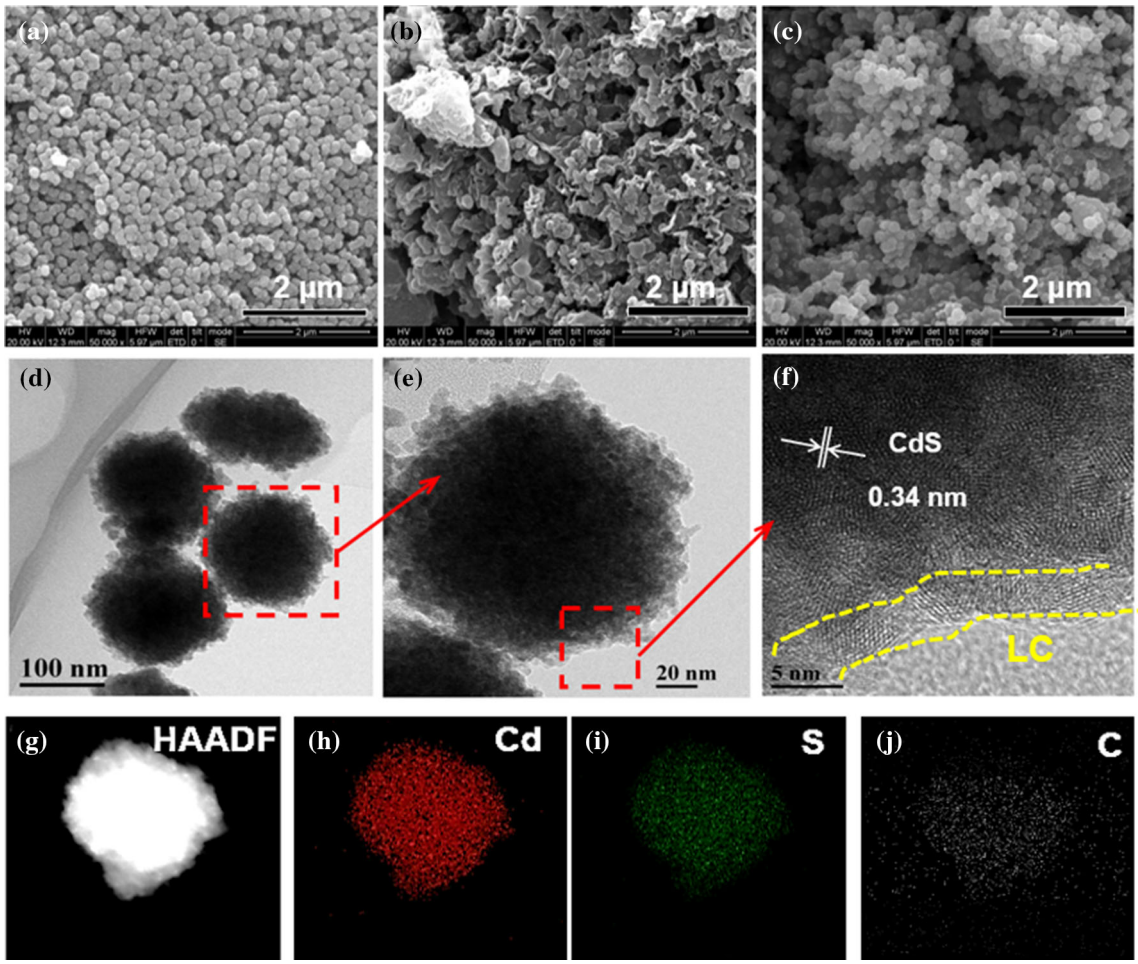

Figure 1 SEM images of **a** CdS, **b** LC and **c** CdS/LC-3 composites; **d**, **e** TEM and **f** HRTEM images of CdS/LC-3; **g**–**j** HAADF and elemental mapping images of CdS/LC-3 composite.

nanoparticles are uniformly dispersed on the attachment surface of the LC and eventually exhibit irregular flowers-like structure, which facilitates dispersing nanoparticles, enhances the active site of the photocatalytic reaction, and further increases the photocatalytic activity. High magnification TEM observations (Fig. 1d, and e) of the CdS/LC-3 composite edges exhibit that CdS nanoparticles with a diameter of approximately 110 nm are well dispersed on the LC. The HRTEM image in Fig. 1f shows the edge of CdS/LC-3 composite, confirming the lattice spacing is determined to be 0.34 nm, which is in line with the (111) plane of CdS [47]. In addition, the HAADF and corresponding elemental mapping images of the CdS/LC-3 composite are also analyzed in Fig. 1g-i and the results revealed that C, S and Cd elements were clearly observed in the synthesized composite photocatalyst.

X-ray photoelectron spectroscopy (XPS) was employed to investigate chemical composition and valence of the elements contained in the CdS/LC-3 composite photocatalyst, as presented in Fig. 2. The XPS full spectrum of CdS/LC-3 in Fig. 2a exhibits five elemental peaks, including C, N, Cd, S and a small amount of O, can be observed. The presence of oxygen mainly comes from the oxygen-containing functional groups on the LC surface. Figure 2b shows the high-resolution spectrum of Cd 3d, corresponding to 405.1 eV (Cd $3d_{5/2}$) and 411.8 eV (Cd $3d_{3/2}$), respectively, indicating the presence of Cd^{2+} in the pure CdS [48]. The S 2p spectrum (Fig. 2c) of the CdS/LC-3 sample possesses two peaks at 161.4 eV and 162.5 eV, which are ascribed to S $2p_{3/2}$ and S $2p_{1/2}$, respectively [49]. High-resolution C 1 s spectra of CdS/LC-3 composite in Fig. 2d reveals that surface functional groups on LC with binding energies at

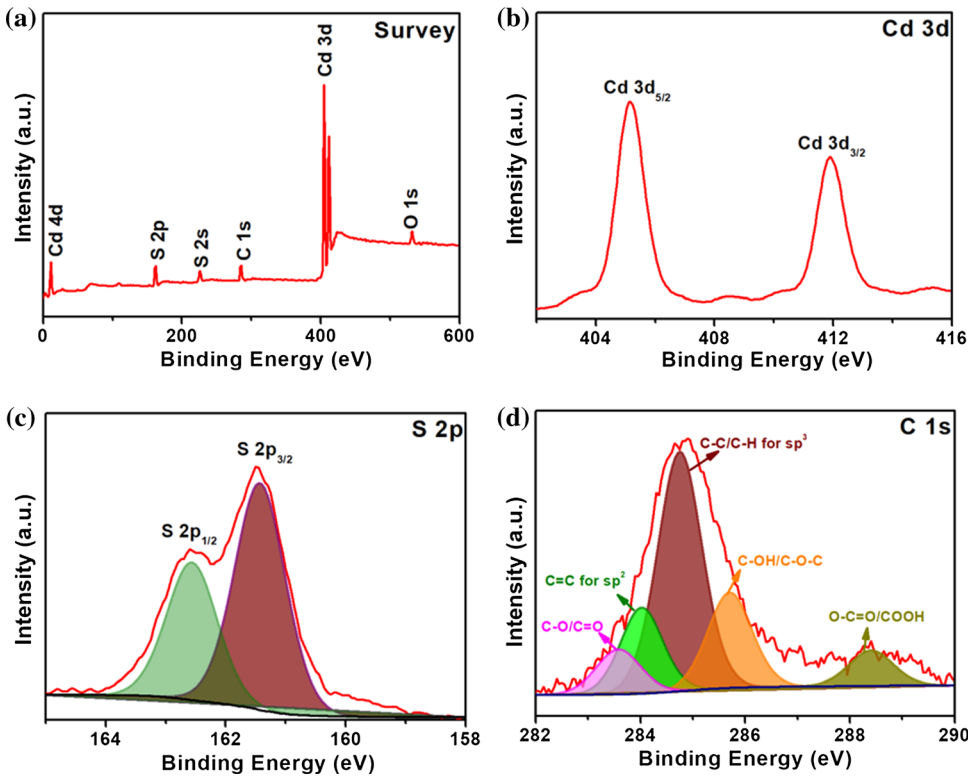

Figure 2 XPS analysis of CdS/LC-3 composite: **a** survey spectrum and high-resolution spectra of **b** Cd 3*d*; **c** S 2*p* and **d** C 1*s*.

288.4 eV, 283.5 eV, and 285.7 eV were observed and attributed to O–C=O/COOH, C–O/C=O, and C–OH/C–O–C bonds, respectively [39]. The remaining binding energies at 284.7 eV and 284 eV (assigning to C–C/C–H for sp^3 and C=C for sp^2) reveal the presence of graphitic structures in LC on the CdS surface [46]. From a typical XPS full spectrum of LC (Fig. S4a), only the C and O peaks are observed, indicating that the structure-directing agent has been completely removed. The C1s high-resolution spectrum of LC (Fig. S4b) shows five binding peaks at 284.6 eV, 285.5 eV, 286.4 eV, 288.3 eV and 288.9 eV, corresponding to sp^2–C, sp^3–C, C–O, C=O and O=C–O, respectively [50]. Among them, the content of sp^2-C has higher peak intensity, indicating a higher degree of graphitization, which is consistent with the Raman results. In addition, XPS analysis shows that the oxygen peak of LC is higher, which indicates that LC contains rich oxygen-containing functional groups. The decomposition of H_2O by thermal template $Mg(OH)_2$ can prevent the excessive pyrolysis of oxygen-containing functional groups [46, 50].

To further investigate the specific surface area and pore structure of as-prepared samples, the samples were characterized by N_2 adsorption–desorption isotherm curves (Fig. 3). The results show that the

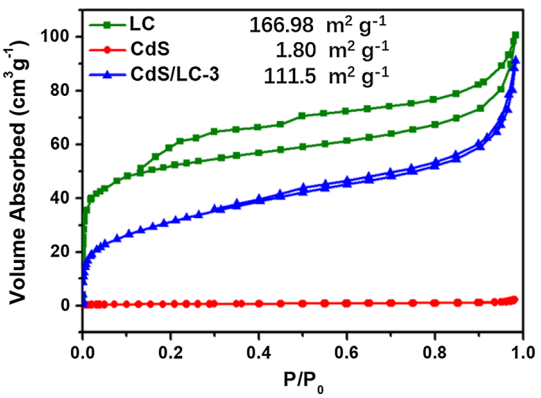

Figure 3 Nitrogen adsorption–desorption isotherm curves and measured specific surface area (inset) of LC, CdS and CdS/LC composite.

isotherms of the LC exhibit a combined i/iv pattern with a narrow H3 hysteresis loop in the range of 0.15–1.0 P/P_0, which is a good indication of the coexistence of micro-, meso- and macro-pores [51, 52]. In addition, it is also observed that the N_2 adsorption–desorption capacity of the pure CdS was quite low, indicating little pore structure in the sample. Due to the addition of LC, the isotherm plot of CdS/LC-3 composite also shows a combined I/IV pattern with a narrower H3 hysteresis loop in the

0.3–1.0 P/P_0 range. The BET surface areas of LC, CdS and CdS/LC-3 samples were measured to be 166.98 $m^2\ g^{-1}$, 1.8 $m^2\ g^{-1}$ and 111.5 $m^2\ g^{-1}$, respectively, indicating that LC can greatly increase the specific surface area of pure CdS and endow CdS nanoparticles with more active sites, which is conducive to boost its photocatalytic performance.

UV–Vis diffuse reflectance spectroscopy (DRS) was carried out to study the optical absorption of LC, pure CdS and CdS/LC-3 composite. As exhibited in Fig. 4a, pristine CdS can absorb solar energy in visible light regions up to 530 nm, and the LC can absorb light well throughout the visible region. Notably, the introduction of LC into CdS leads to an increase in visible light absorption. This is because the LC is black, which effectively reduces the reflection of light and thus increases the absorption of pristine CdS (digital photographs of as-prepared samples in Fig. S5), which indicates that LC can act as a photosensitizer to promote the production and transfer of photo-induced electrons under visible light irradiation. Furthermore, the band gap energy (E_g) value of the prepared CdS was measured to be 2.47 eV in Fig. 4b.

The photooxidation activity for photodegradation of ciprofloxacin (CIP) by the CdS/LC composite photocatalysts under visible light was evaluated and is illustrated in Fig. 5. In Fig. 5a, the photodegradation curve in the absence of photocatalyst clearly demonstrates that the structure of CIP is very stable against photodegradation. Furthermore, from the adsorption–desorption equilibrium curves of all samples, it can be seen that the adsorption capacity of the CdS/LC composites for CIP was much higher than that of CdS due to the superior adsorption capacity of LC. As the amount of LC gradually increases in the composite system (from CdS/LC-1 to CdS/LC-3), the photocatalytic degradation activity is gradually enhanced due to the excellent electron transport properties of LC that promotes the photo-induced electron transfer of CdS and subsequently enhances the photocatalytic activity [53]. Most importantly, the CdS/LC-3 sample showed excellent photocatalytic performance for the degradation of CIP, with the degradation efficiency of the CdS/LC-3 sample reaching a high value of 98% within 60 min irradiation. It can be found that excess LC reduces the photocatalytic performance of the photocatalyst, probably because the covered numerous LC hinders the utilization of visible light at the active site of the photocatalyst [54]. Therefore, an appropriate ratio of composite photocatalyst (CdS/LC-3) can exhibit improved adsorption activity and photocatalytic activity. Figure 5b shows the corresponding pseudo-first-order kinetic plots for the prepared photocatalysts during the CIP photodegradation. It can be seen from the plots that all samples showed good linearity, indicating that all photocatalysts followed the pseudo-first-order kinetics, and the slope of the CdS/LC-3 sample was maximum. Based on the corresponding kinetic constants (k) of the samples (Fig. 5c), it is evident that k value of the CdS/LC-3 is about 2.3 times higher than bare CdS. In order to investigate the stable performance and recyclability of composite, the photocatalytic cycling performance of CdS/LC-3 was tested and is shown in Fig. 5d. It was found that the photocatalytic activity of CdS/LC-3 was very stable after four consecutive degradation cycles, which also indicated that the addition of the LC sample successfully inhibited the photocorrosion and agglomeration of CdS in the photocatalytic reaction.

To further investigate the photoreduction activity of CdS/LC composite, photocatalytic hydrogen

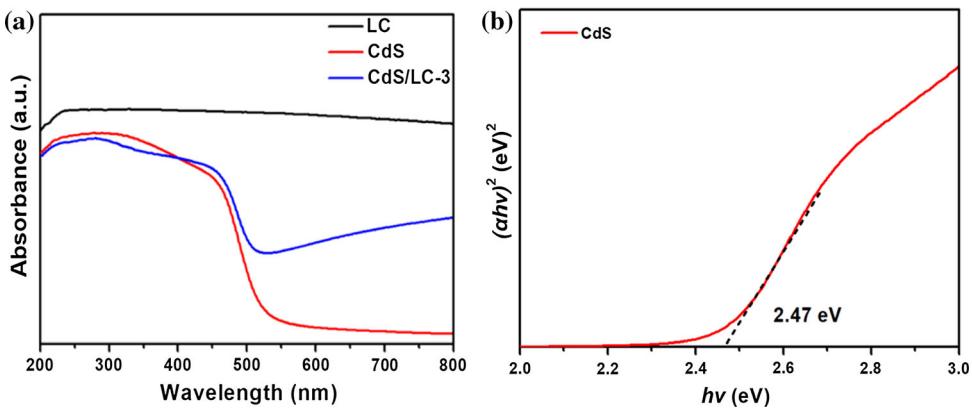

Figure 4 **a** UV diffuse reflectance spectra (DRS) of LC, CdS and CdS/LC-3 and **b** measured energy band gap of CdS.

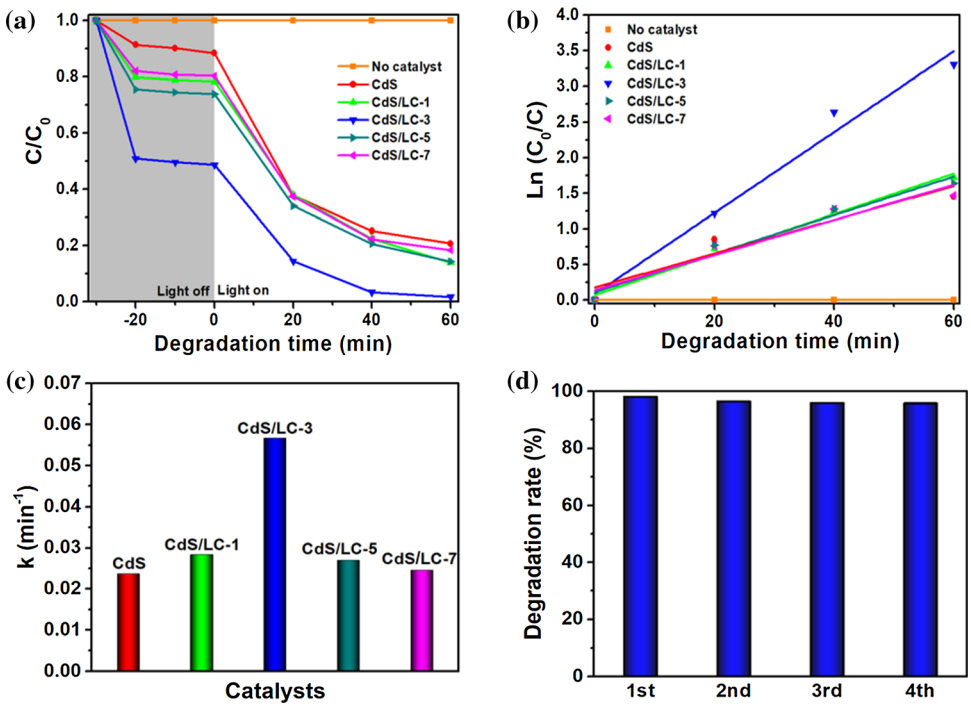

Figure 5 **a** Photocatalytic degradation curves of CIP over as-prepared photocatalysts under visible light irradiation ($\lambda > 420$ nm, 0.3 g L^{-1} catalyst, 50 mg L^{-1} CIP). **b** Pseudo-first-order reaction kinetic curves and **c** reaction constants of photocatalytic degradation of CIP by different samples under visible light irradiation ($\lambda > 420$ nm, 0.3 g L^{-1} catalyst, 50 mg L^{-1} CIP). **d** Recycle photocatalytic degradation experiments of CdS/LC-3 ($\lambda > 420$ nm, 0.3 g L^{-1} catalyst, 50 mg L^{-1} CIP).

production experiments with CdS/LC photocatalysts were carried out. As shown in Fig. 6a, it can be seen that the amount of hydrogen production increased for all samples with increasing visible light irradiation time, which proves that this is indeed a photocatalytic reaction. Moreover, it can be noted that the hydrogen production of pure CdS is very low (62.9 μmol in 4 h). After coating CdS on the LC to form CdS/LC composite, photocatalytic performance of as-prepared samples has been enhanced, indicating that LC plays an indispensable role in this composite photocatalytic system. It is worth noting that the highest photocatalytic performance of the CdS/LC-3 composite (234.7 μmol in 4 h) was observed, which was about 3.73 times higher than that of CdS. It is clear that the excess LC reduces the hydrogen production of the photocatalyst, which may also be due to the large amount of LC covering the photocatalyst, hindering the visible light from the active sites of the photocatalyst, thus reducing the hydrogen production efficiency [55–58]. It can be found that the photocatalytic hydrogen production and TC degradation activity of CdS/LC-3 is higher than most reported photocatalysts in Table S1. In addition, as exhibited in Fig. 6b, the CdS/LC-3 composite showed excellent stability over four cycle tests (4 h of exposure to visible light each time). For investigating the charge separation of as-prepared samples, the photoluminescence (PL) spectra of CdS and CdS/LC-3 composite were recorded at an excitation wavelength of 325 nm and are shown in Fig. S6a. In general, the lower the PL intensity, the stronger the separation

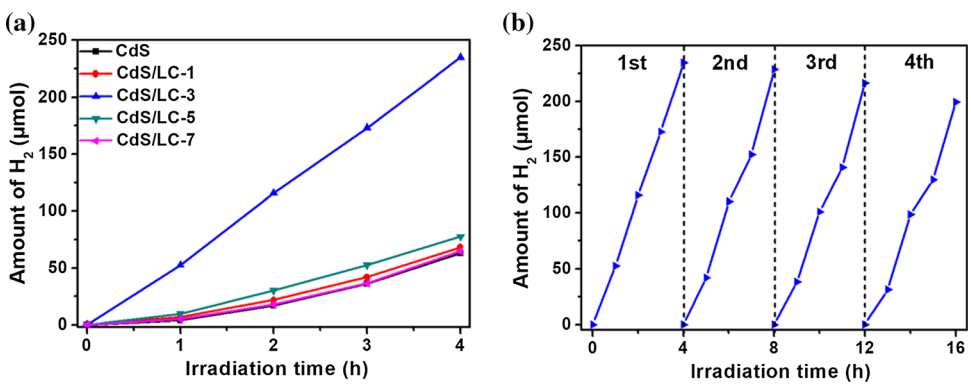

Figure 6 **a** Photocatalytic H_2 production curves of as-prepared samples under visible light irradiation ($\lambda > 420$ nm, 0.3 g L^{-1} catalyst). **b** Cycling stability tests for photocatalytic H_2 production over CdS/LC-3 composite photocatalyst.

efficiency of electron–hole pairs of photocatalytic materials. CdS exhibits a strong intrinsic emission band with a peak at around 500 nm, and the PL strength of CdS/LC-3 composite is greatly reduced compared with that of pristine CdS, probably because the combination of LC and CdS can promote the separation of photo-generated carriers [59–62]. Time-resolved fluorescence spectroscopy was used to furthermore measure and calculate the lifetime of the charge carriers over the as-prepared photocatalysts. As presented in Fig. S6b, from the time-resolved fluorescence decay fitting curves, it can be obtained that the average lifetime (τ_{ave}) of CdS is 4.93 ns. In contrast, CdS/LC-3 exhibits longer lifetime of 9.01 ns, implying that the addition of LC could promote the charge transfer separation efficiency. In addition, as a tool to study the interfacial electron transport and charge transfer on the photocatalyst, photoelectrochemical measurements were performed. In Fig. S6c, it can be seen that the photocurrent responses of the as-obtained photocatalysts were generated immediately after visible light irradiation and then reached a maximum value, and when the light was turned off, the photocurrent disappeared rapidly, confirming it is indeed a photocatalytic reaction process. And CdS/LC-3 exhibited a photocurrent density about twice that of pure CdS, which is consistent with the above PL results, further demonstrating that LC plays an important role in suppressing the recombination of electron–hole pairs and improving the separation efficiency of photogenerated electrons at the composite interface [63, 64]. Furthermore, electrochemical impedance spectroscopy (EIS) was performed to measure the charge transfer resistance of as-prepared photocatalysts. As presented in Fig. S6d, the CdS/LC-3 composite exhibited a much smaller semicircle diameter than pure CdS, indicating faster charge transfer occurred at their interfaces in the composite after the introduction of LC [65–70]. These evidences show that the addition of LC greatly enhances the transfer of photoinduced electrons, promotes the photocatalytic reaction and plays an active role in photo-induced carrier separation.

To investigate the main reactive active species, benzoquinone (BQ), isopropanol (IPA) and triethanolamine (TEOA) were used as the trapping agents of $\bullet O_2^-$,•OH and h^+, respectively, during the photocatalytic reaction (Fig. S7a and b). During the photocatalytic reaction, the photodegradation rate of CIP over CdS and CdS/LC-3 samples decreased significantly with the addition of BQ, indicating that $\bullet O_2^-$ radicals were the most active species in this study. In addition, the degradation rates of CIP over CdS and CdS/LC-3 samples were also limited after the addition of IPA and TEOA, indicating that •OH and h^+ are also as the reactive species participating in the photocatalytic reaction. The reactive oxygen species of CdS and CdS/LC-3 composites were investigated using the Electron spin resonance (ESR) method in the presence of dimethyl pyridine N-oxide (DMPO) free radical trapping agents (Fig. S7c and d). In the dark, neither $\bullet O_2^-$ nor •OH signals of CdS and CdS/LC-3 were observed. Significantly, under visible light irradiation, the $\bullet O_2^-$ and •OH signals of both CdS and CdS/LC-3 were clearly detected and the signal intensities of CdS/LC are significantly stronger than those of the pure CdS. Hence, the results also indicate that the CdS/LC-3 composite is more efficient in terms of separation efficiency of photogenerated carriers compared with pure CdS [46]. According to the Mott–Schottky plot in Fig. S8, the derived flat-band potential is around − 0.60 V vs. Ag/AgCl for pristine CdS, i.e., − 0.40 V vs. NHE (pH = 6.5). Thus, the CB of CdS is measured to be -0.43 V vs. NHE (pH = 7). Due to the bandgap of 2.47 eV, the VB of CdS is located at 2.04 V. Based on the above results, the photocatalytic enhancement mechanism of CdS/LC composite is proposed as shown in Fig. 7. The CdS nanoparticles can be homogeneously immobilized on the LC and the CdS/LC composite exhibits a hierarchical structure similar to the three-dimensional nanostructure of LC, which can confer fast matter transfer and enhanced light-harvesting properties to the photocatalyst. In addition, the three-dimensional nanostructure of LC provides a large number of adsorption sites for capturing the reaction substrate. More importantly, the interfacial electronic interactions between LC and CdS expand the light absorption range and promote the photogenerated carrier separation of CdS. When visible light is irradiated onto the composite, electrons (e^-) are excited from the valence band (VB) of CdS to the conduction band (CB), while holes (h^+) are left behind. Generally, most of the e^- and h^+ recombine quickly without participating in any chemical reactions, resulting in low reactivity [71]. Fortunately, LC with abundant sp^2 hybridized carbon atoms is highly efficient in storing and shuttling electrons, and the photoexcited e^- in CdS is transferred to LC due to the intimate contact between CdS

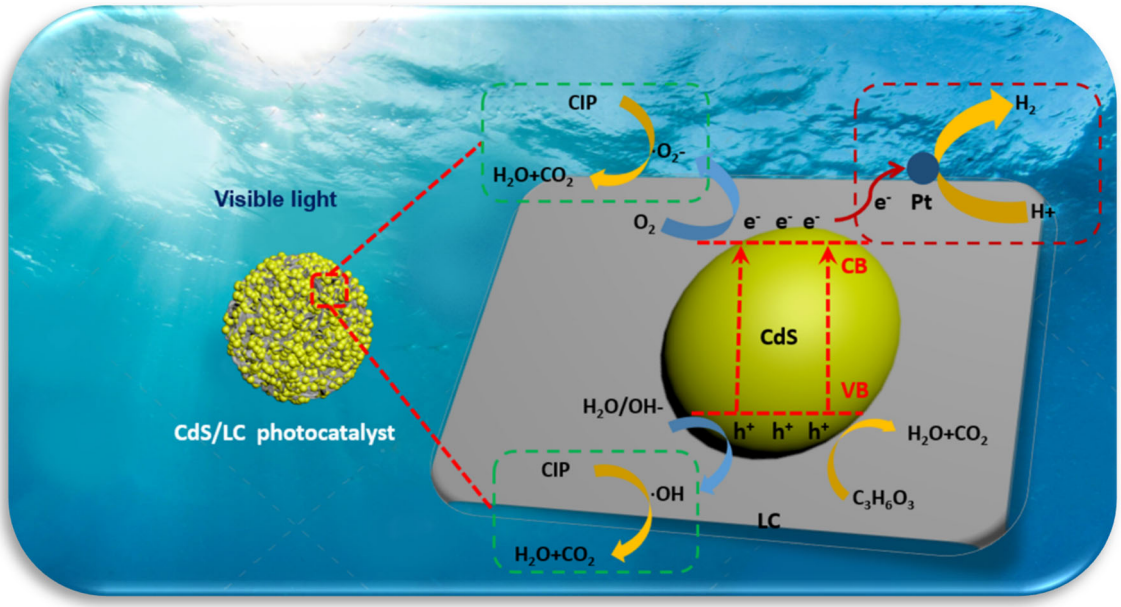

Figure 7 Possible mechanism for photocatalytic degradation of CIP and H_2 evolution over CdS/LC composite photocatalyst.

[72]. During photodegradation, h^+ in VB could react with H_2O or OH^- to form •OH, and e^- on CB are easily to react with O_2 absorbed on its surface to form $\bullet O_2^-$. •OH and $\bullet O_2^-$ are also involved in the oxidation reaction of CIP [46]. On the other hand, in the photocatalytic hydrogen production process, e^- in the composite could react with H^+ through the co-catalyst Pt nanoparticles to produce H_2 [73–75], while h^+ in the VB can react with lactic acid to produce H_2O and CO_2 [5, 76–79]. Combining several important advantages, the CdS/LC composite presents excellent photocatalytic efficiency for the photodegradation of CIP and the evolution of photocatalytic H_2.

Conclusion

To sum up, LC with irregular flower-like structure was prepared by simple carbonization method, and then the uniform fixation of CdS nanoparticles in LC was achieved by in situ growth. Due to the interfacial electronic interactions between CdS and LC, the CdS/LC composite photocatalyst exhibits extended optical absorption and enhanced photogenerated carrier separation. In addition, the irregular flower-like structure has multiple advantages such as layered structure providing high mass transfer efficiency, enhanced light-harvesting capability and good stability. Therefore, the CdS/LC composites exhibit excellent photocatalytic efficiency and recyclability for the photodegradation of CIP (98% within 60 min irradiation) and photocatalytic hydrogen evolution (234.7 μmol in 4 h) compared to pristine CdS. This study LC was cleverly designed and fabricated to address the shortcomings of CdS, providing a feasible strategy for the practical application of CdS. This research work provides a novel available pathway for lignin utilization, enabling high-quality utilization of lignin.

Acknowledgements

The authors would like to acknowledge the funding support from the National Natural Science Foundation of China (Nos. 21906072, 22006057 and 31971616), the Natural Science Foundation of Jiangsu Province (BK20190982), Henan Postdoctoral Foundation (202003013), "Doctor of Mass entrepreneurship and innovation" Project in Jiangsu Province, Doctoral Scientific Research Foundation of Jiangsu University of Science and Technology (China) (1062931806 and 1142931803), the Science and Technology Innovation Development Plan of Jilin City (201830811), Science Development Project of Jilin City (20190104056), the Natural Science Foundation Project of Jilin Provincial Science and Technology Development Plan (20190201277JC), the Science and

Technology Research Project of the Department of Education of Jilin Province (JJKH20200039KJ) and the Science and Technology Research Project of Jilin City (20190104120)

Supplementary Information: The online version contains supplementary material available at https://doi.org/10.1007/s10853-021-06589-4.

References

[1] Guo F, Shi W, Li M, Shi Y, Wen H (2019) 2D/2D Z-scheme heterojunction of $CuInS_2$/g-C_3N_4 for enhanced visible-light-driven photocatalytic activity towards the degradation of tetracycline. Sep Purif Technol 210:608–615

[2] Shi W, Guo F, Li M, Shi Y, Wu M, Tang Y (2019) Enhanced visible-light-driven photocatalytic H2 evolution on the novel nitrogen-doped carbon dots/$CuBi_2O_4$ microrods composite. J Alloy Compd 775:511–517

[3] Budnyak T, Onwumere J, Pylypchuk I, Jaworski A, Chen J, Rokicinska A, Lindstrom M, Kustrowski P, Sevastyanova O, Slabon A (2021) LignoPhot: Conversion of hydrolysis lignin into the photoactive hybrid lignin/$B_{i4}O_5Br_2$/BiOBr composite for simultaneous dyes oxidation and Co^{2+} and Ni^{2+} recycling. Chemosphere 279:130538

[4] Shi W, Guo F, Li M, Shi Y, Shi M, Yan C (2019) Constructing 3D sub-micrometer CoO octahedrons packed with layered MoS_2 shell for boosting photocatalytic overall water splitting activity. Appl Surf Sci 473:928–933

[5] Shi W, Guo F, Li M, Shi Y, Tang Y (2019) N-doped carbon dots/CdS hybrid photocatalyst that responds to visible/near-infrared light irradiation for enhanced photocatalytic hydrogen production. Sep Purif Technol 212:142–149

[6] Onwumere J, Pictek J, Budnyak T, Chen J, Budnyk S, Karim Z, Thersleff T, Kuśtrowski P, Mathew A, Slabon A (2020) CelluPhot: hybrid cellulose-bismuth oxybromide membrane for pollutant removal. ACS Appl Mater Inter 12:42891–42901

[7] Shi W, Li M, Huang X, Ren H, Yan C, Guo F (2020) Facile synthesis of 2D/2D $Co_3(PO_4)_2$/g-C_3N_4 heterojunction for highly photocatalytic overall water splitting under visible light. Chem Eng J 382:122960

[8] Shi W, Wang J, Yang S, Lin X, Guo F, Shi J (2020) Fabrication of a ternary carbon dots/CoO/g-C_3N_4 nanocomposite photocatalyst with enhanced visible-light-driven photocatalytic hydrogen production. J Chem Technol Biotechnol 95:2129–2138

[9] Martindale BCM, Hutton GAM, Caputo CA, Prantl S, Godin R, Durrant JR, Reisner E (2017) Enhancing light absorption and charge transfer efficiency in carbon dots through graphitization and core nitrogen doping. Angew Chem Int Ed 56:6459–6463

[10] Xu X, Ding X, Yang XL, Wang P, Li S, Lu ZX, Chen H (2019) Oxygen vacancy boosted photocatalytic decomposition of ciprofloxacin over Bi2MoO6: Oxygen vacancy engineering, biotoxicity evaluation and mechanism study. J Hazard Mater 364:691–699

[11] Zhang YQ, Pan HQ, Zhang FG (2019) Solvothermal synthesis of CDs/Bi_4O_5Br 2 nanocomposites with improved visible-light photocatalytic ciprofloxacin (CIP) decontamination. Mater Lett 251:114–117

[12] Guo F, Li M, Ren H, Huang X, Hou W, Wang C, Shi W, Lu C (2019) Fabrication of p-n $CuBi_2O_4/MoS_2$ heterojunction with nanosheets-on-microrods structure for enhanced photocatalytic activity towards tetracycline degradation. Appl Surf Sci 491:88–94

[13] Guo F, Li M, Ren H, Huang X, Shu K, Shi W, Lu C (2019) Facile bottom-up preparation of Cl-doped porous g-C_3N_4 nanosheets for enhanced photocatalytic degradation of tetracycline under visible light. Sep Purif Technol 228:115770

[14] Zhu Z, Lu Z, Wang D, Tang X, Yan Y, Shi W, Wang Y, Gao N, Yao X, Dong H (2016) Construction of high-dispersed Ag/Fe_3O_4/g-C_3N_4 photocatalyst by selective photo-deposition and improved photocatalytic activity. Appl Catal B: Environ 182:115–122

[15] Lu CY, Guo F, Yan QZ, Zhang ZJ, Li D, Wang LP, Zhou YH (2019) Hydrothermal synthesis of type II $ZnIn_2S_4/BiPO_4$ heterojunction photocatalyst with dandelion-like microflower structure for enhanced photocatalytic degradation of tetracycline under simulated solar light. J Alloy Compd 811:151976

[16] Shi W, Li M, Ren H, Guo F, Huang X, Shi Y, Tang Y (2019) Construction of a 0D/1D composite based on Au nanoparticles/$CuBi_2O_4$ microrods for efficient visible-light-driven photocatalytic activity. Beilstein J Nanotechnol 10:1360–1367

[17] Guo F, Huang X, Chen Z, Ren H, Li M, Chen L (2020) MoS_2 nanosheets anchored on porous $ZnSnO_3$ cubes as an efficient visible-light-driven composite photocatalyst for the degradation of tetracycline and mechanism insight. J Hazard Mater 390:122158

[18] Shi W, Li M, Huang X, Ren H, Guo F, Tang Y, Lu C (2020) Construction of $CuBi_2O_4/Bi_2MoO_6$ p-n heterojunction with nanosheets-on-microrods structure for improved photocatalytic activity towards broad-spectrum antibiotics degradation. Chem Eng J 394:125009

[19] Zhu Q, Sun Y, Na F, Wei J, Xu S, Li Y, Guo F (2019) Fabrication of CdS/titanium-oxo-cluster nanocomposites based on a Ti_{32} framework with enhanced photocatalytic activity for tetracycline hydrochloride degradation under visible light. Appl Catal B: Environ 254:541–550

[20] Wu X, Zhao J, Wang L, Han M, Zhang M, Wang H, Huang H, Liu Y, Kang Z (2017) Carbon dots as solid-state electron mediator for $BiVO_4$/CDs/CdS Z-scheme photocatalyst working under visible light. Appl Catal B: Environ 206:501–509

[21] Li Q, Guo B, Yu J, Ran J, Zhang B, Yan H, Gong JR (2011) Highly efficient visible-light-driven photocatalytic hydrogen production of CdS-cluster-decorated graphene nanosheets. J Am Chem Soc 133:10878–10884

[22] Cai Q, Hu Z, Zhang Q, Li B, Shen Z (2017) Fullerene (C_{60})/CdS nanocomposite with enhanced photocatalytic activity and stability. Appl Surf Sci 403:151–158

[23] Wang P, Zhang J, He H, Xu X, Jin Y (2015) The important role of surface ligand on CdSe/CdS core/shell nanocrystals in affecting the efficiency of H_2 photogeneration from water. Nanoscale 7:5767–5775

[24] Liu Q, Shang Q, Khalil A, Fang Q, Chen S, He Q, Xiang T, Liu D, Zhang Q, Luo Y, Song L (2016) In situ integration of a metallic 1T-MoS_2/CdS heterostructure as a means to promote visible-light-driven photocatalytic hydrogen evolution. ChemCatChem 8:2614–2619

[25] Hu Y, Gao X, Yu L, Wang Y, Ning J, Xu S, Lou XW (2013) Carbon-coated CdS petalous nanostructures with enhanced photostability and photocatalytic activity. Angew Chem Int Ed 52:5636–5639

[26] Kumar A, Sharma G, Naushad M, Al-Muhtaseb A, García-Peñas A, Mola GT, Si C, Stadler FJ (2020) Bio-inspired and biomaterials-based hybrid photocatalysts for environmental detoxification: a review. Chem Eng J 382:122937

[27] Wan Z, Sun Y, Tsang DCW, Khan E, Yip ACK, Ng YH, Rinklebe J, Ok YS (2020) Customised fabrication of nitrogen-doped biochar for environmental and energy applications. Chem Eng J 401:126136

[28] Li H, Wang H, Guo J, Ye S, Shi W, Peng X, Song J, Qu J (2020) Long-wavelength excitation of carbon dots as the probe for real-time imaging of the living-cell cycle process. Sensors Actuat B: Chem 311:127891

[29] Shi W, Ren H, Huang X, Li M, Tang Y, Guo F (2020) Low cost red mud modified graphitic carbon nitride for the removal of organic pollutants in wastewater by the synergistic effect of adsorption and photocatalysis. Sep Purif Technol 237:116477

[30] Bi Z, Kong Q, Cao Y, Sun G, Su F, Wei X, Li X, Ahmad A, Xie L, Chen C-M (2019) Biomass-derived porous carbon materials with different dimensions for supercapacitor electrodes: a review. J Mater Chem A 7:16028–16045

[31] Cui J, Zhang F, Li H, Cui J, Ren Y, Yu X (2020) Recent Progress in biochar-based photocatalysts for wastewater treatment: synthesis, mechanisms, and applications. Appl Sci 10:1019

[32] Chen X, Kuo D-H, Lu D, Hou Y, Kuo Y-R (2016) Synthesis and photocatalytic activity of mesoporous TiO_2 nanoparticle using biological renewable resource of un-modified lignin as a template. Micropor Mesopor Mater 223:145–151

[33] Wang H, Qiu X, Liu W, Yang D (2017) Facile preparation of well-combined lignin-based carbon/ZnO hybrid composite with excellent photocatalytic activity. Appl Surf Sci 426:206–216

[34] Srisasiwimon N, Chuangchote S, Laosiripojana N, Sagawa T (2018) TiO_2/lignin-based carbon composited photocatalysts for enhanced photocatalytic conversion of lignin to high value chemicals. ACS Sustain Chem Eng 6:13968–13976

[35] Khan A, Nair V, Colmenares JC, Glaser R (2018) Lignin-based composite materials for photocatalysis and photovoltaics. Top Curr Chem (Cham) 376:20

[36] Granone LI, Sieland F, Zheng N, Dillert R, Bahnemann DW (2018) Photocatalytic conversion of biomass into valuable products: a meaningful approach? Green Chem 20:1169–1192

[37] Deng J, Xiong T, Xu F, Li M, Han C, Gong Y, Wang H, Wang Y (2015) Inspired by bread leavening: one-pot synthesis of hierarchically porous carbon for supercapacitors. Green Chem 17:4053–4060

[38] Xue Y, Chang Q, Hu X, Cai J, Yang H (2020) A simple strategy for selective photocatalysis degradation of organic dyes through selective adsorption enrichment by using a complex film of CdS and carboxylmethyl starch. J Environ Manage 274:111184

[39] Xiang Z, Nan J, Deng J, Shi Y, Zhao Y, Zhang B, Xiang X (2019) Uniform CdS-decorated carbon microsheets with enhanced photocatalytic hydrogen evolution under visible-light irradiation. J Alloy Compd 770:886–895

[40] Zhang B, Yang D, Wang H, Qian Y, Huang J, Yu L, Qiu X (2018) Activation of enzymatic hydrolysis lignin by NaOH/urea aqueous solution for enhancing its sulfomethylation reactivity. ACS Sustain Chem Eng 7:1120–1128

[41] Xi Y, Yang D, Qiu X, Wang H, Huang J, Li Q (2018) Renewable lignin-based carbon with a remarkable electrochemical performance from potassium compound activation. Ind Crop Prod 124:747–754

[42] Gao H, Mo Z, Guo R, Niu X, Li Z (2018) Formation of snowflake-like CdS/reduced graphene oxide composite for efficient photocatalytic organic dye degradation. J Mater Sci: Mater El 29:5944–5953

[43] Zubair M, Vanhaecke EMM, Svenum I-H, Rønning M, Yang J (2020) Core-shell particles of C-doped CdS and graphene: a noble metal-free approach for efficient photocatalytic H_2 generation. Green Energy Environ 5:461–472

[44] Ma L, Liu M, Jing D, Guo L (2015) Photocatalytic hydrogen production over CdS: effects of reaction atmosphere studied by in situ Raman spectroscopy. J Mater Chem A 3:5701–5707

[45] Donar YO, Bilge S, Sinağ A (2020) Utilisation of lignin as a model biomass component for preparing a highly active photocatalyst under UV and visible light. Mater Sci Semicon Proc 118:105151

[46] Zhang B, Yang D, Qiu X, Qian Y, Wang H, Yi C, Zhang D (2020) Fabricating ZnO/lignin-derived flower-like carbon composite with excellent photocatalytic activity and recyclability. Carbon 162:256–266

[47] Wang Y, Chen J, Liu L, Xi X, Li Y, Geng Z, Jiang G, Zhao Z (2019) Novel metal doped carbon quantum dots/CdS composites for efficient photocatalytic hydrogen evolution. Nanoscale 11:1618–1625

[48] Lin Y, Pan D, Luo H (2021) Hollow direct Z-scheme CdS/BiVO4 composite with boosted photocatalytic performance for RhB degradation and hydrogen production. Mater Sci Semicon Proc 121:105453

[49] Qin Y, Li H, Lu J, Meng F, Ma C, Yan Y, Meng M (2020) Nitrogen-doped hydrogenated TiO_2 modified with CdS nanorods with enhanced optical absorption, charge separation and photocatalytic hydrogen evolution. Chem Eng J 384:123275

[50] Zhang B, Yang D, Qian Y, Pang Y, Li Q, Qiu X (2020) Engineering a lignin-based hollow carbon with opening structure for highly improving the photocatalytic activity and recyclability of ZnO. Ind Crop Prod 155:112773

[51] Cui X, Wang Y, Jiang G, Zhao Z, Xu C, Duan A, Liu J, Wei Y, Bai W (2014) The encapsulation of CdS in carbon nanotubes for stable and efficient photocatalysis. J Mater Chem A 2:20939–20946

[52] Shi W, Shu K, Sun H, Ren H, Li M, Chen F, Guo F (2020) Dual enhancement of capturing photogenerated electrons by loading CoP nanoparticles on N-deficient graphitic carbon nitride for efficient photocatalytic degradation of tetracycline under visible light. Sep Purif Technol 246:116930

[53] Shi W, Guo F, Wang H, Han M, Li H, Yuan S, Huang H, Liu Y, Kang Z (2017) Carbon dots decorated the exposing high-reactive (111) facets CoO octahedrons with enhanced photocatalytic activity and stability for tetracycline degradation under visible light irradiation. Appl Catal B: Environ 219:36–44

[54] Shi W, Lv H, Yuan S, Huang H, Liu Y, Kang Z (2017) Synergetic effect of carbon dots as co-catalyst for enhanced photocatalytic performance of methyl orange on $ZnIn_2S_4$ microspheres. Sep Purif Technol 174:282–289

[55] Shi W, Guo F, Zhu C, Wang H, Li H, Huang H, Liu Y, Kang Z (2017) Carbon dots anchored on octahedral CoO as a stable visible-light-responsive composite photocatalyst for overall water splitting. J Mater Chem A 5:19800–19807

[56] Guo F, Sun H, Cheng L, Shi W (2020) Oxygen-defective ZnO porous nanosheets modified by carbon dots to improve their visible-light photocatalytic activity and gain mechanistic insight. New J Chem 44:11215–11223

[57] Guo F, Huang X, Chen Z, Sun H, Shi W (2020) Investigation of visible-light-driven photocatalytic tetracycline degradation via carbon dots modified porous $ZnSnO_3$ cubes: Mechanism and degradation pathway. Sep Purif Technol 253:117518

[58] Shi W, Yang S, Sun H, Wang J, Lin X, Guo F, Shi J (2020) Carbon dots anchored high-crystalline g-C3N4 as a metal-free composite photocatalyst for boosted photocatalytic degradation of tetracycline under visible light. J Mater Sci 56:2226–2240

[59] Liu Y, Yu Y-X, Zhang W-D (2013) Carbon quantum dots-doped CdS microspheres with enhanced photocatalytic performance. J Alloy Compd 569:102–110

[60] Liu Y, Liu C, Shi C, Sun W, Lin X, Shi W, Hong Y (2021) Carbon-based quantum dots (QDs) modified ms/tz-BiVO4 heterojunction with enhanced photocatalytic performance for water purification. J Alloy Compd 881:160437

[61] Pan J, Guo F, Sun H, Li M, Zhu X, Gao L, Shi W (2021) Nanodiamond decorated 2D hexagonal Fe2O3 nanosheets with a Z-scheme photogenerated electron transfer path for enhanced photocatalytic activity. J Mater Sci 56:6663–6675

[62] Pan J, Guo F, Sun H, Shi Y, Shi W (2021) Nanodiamonds anchored on porous ZnSnO3 cubes as an efficient composite photocatalyst with improved visible-light photocatalytic degradation of tetracycline. Sep Purif Technol 263:118398

[63] Quan F, Zhang J, Li D, Zhu Y, Wang Y, Bu Y, Qin Y, Xia Y, Komarneni S, Yang D (2018) Biomass as a template leads to CdS@Carbon aerogels for efficient photocatalytic hydrogen Evolution and stable photoelectrochemical cells. ACS Sustain Chem Eng 6:14911–14918

[64] Sun W, Yang S, Liu Y, Shi C, Shi W, Lin X, Guo F, Hong Y (2021) Fabricating nitrogen-doped carbon dots (NCDs) on $Bi_{3.64}Mo_{0.36}O_{6.55}$ nanospheres: a nanoheterostructure for enhanced photocatalytic performance for water purification. J Phys Chem Solids 159:110283

[65] Zhang L, Huang L, Jiang X, Li J, Sun X (2020) Efficient porous carbon/CdS composite photocatalyst for dye degradation. J Mater Sci: Mater El 32:337–346

[66] Shi W, Li M, Huang X, Ren H, Guo F, Yan C (2020) Three-dimensional Z-Scheme $Ag_3PO_4/Co_3(PO_4)_2$@Ag

heterojunction for improved visible-light photocatalytic degradation activity of tetracycline. J Alloy Compd 818:152883

[67] Shi W, Liu C, Li M, Lin X, Guo F, Shi J (2020) Fabrication of ternary $Ag_3PO_4/Co_3(PO_4)_2/g\text{-}C_3N_4$ heterostructure with following Type II and Z-Scheme dual pathways for enhanced visible-light photocatalytic activity. J Hazard Mater 389:121907

[68] Liu E, Lin X, Hong Y, Yang L, Luo B, Shi W, Shi J (2021) Rational copolymerization strategy engineered C self-doped g-C3N4 for efficient and robust solar photocatalytic H_2 evolution. Renew Energ 178:757–765

[69] Guo F, Chen Z, Huang X, Cao L, Cheng X, Shi W, Chen L (2021) Cu3P nanoparticles decorated hollow tubular carbon nitride as a superior photocatalyst for photodegradation of tetracycline under visible light. Sep Purif Technol 275:119223

[70] Guo F, Wang L, Sun H, Li M, Shi W (2020) High-efficiency photocatalytic water splitting by a N-doped porous $g\text{-}C_3N_4$ nanosheet polymer photocatalyst derived from urea and N, N-dimethylformamide. Inorg Chem Front 7:1770–1779

[71] Chai Y-Y, Qu D-P, Ma D-K, Chen W, Huang S (2018) Carbon quantum dots/Zn^{2+} ions doped-CdS nanowires with enhanced photocatalytic activity for reduction of 4-nitroaniline to p-phenylenediamine. Appl Surf Sci 450:1–8

[72] Chen Z, Feng C, Li W, Sun Z, Hou J, Li X, Xu L, Sun M, Bu Y (2018) Enhanced visible-light-driven photocatalytic activities of 0D/1D heterojunction carbon quantum dot modified CdS nanowires. Chin J Catal 39:841–848

[73] Wang Q, Lian J, Ma Q, Zhang S, He J, Zhong J, Li J, Huang H, Su B (2017) Preparation of carbon spheres supported CdS photocatalyst for enhancement its photocatalytic H_2 evolution. Catal Today 281:662–668

[74] Guo F, Wang L, Sun H, Li M, Shi W, Lin X (2020) A one-pot sealed ammonia self-etching strategy to synthesis of N-defective $g\text{-}C_3N_4$ for enhanced visible-light photocatalytic hydrogen. Int J Hydrogen Energ 45:30521–30532

[75] Guo F, Huang X, Chen Z, Shi Y, Sun H, Cheng X, Shi W, Chen L (2021) Formation of unique hollow $ZnSnO_3$@-$ZnIn_2S_4$ core-shell heterojunction to boost visible-light-driven photocatalytic water splitting for hydrogen production. J Colloid Interface Sci 602:889–897

[76] Guo J, Yang C, Sun Z, Yang Z, Wang L, Lu C, Ma Z, Guo F (2020) Ternary $Fe_3O_4/MoS_2/BiVO_4$ nanocomposites: novel magnetically separable visible light-driven photocatalyst for efficiently degradation of antibiotic wastewater through p–n heterojunction. J Mater Sci: Mater El 31:16746–16758

[77] Wang L, Guan R, Qi Y, Zhang F, Li P, Wang J, Qu P, Zhou G, Shi W (2021) Constructing Zn-P charge transfer bridge over $ZnFe_2O_4$-black phosphorus 3D microcavity structure: Efficient photocatalyst design in visible-near-infrared region. J Colloid Interface Sci 600:463–472

[78] Zhang W, Shi W, Sun H, Shi Y, Luo H, Jing S, Fan Y, Guo F, Lu C (2021) Fabrication of ternary $CoO/g\text{-}C_3N_4/Co_3O_4$ nanocomposite with p-n-p type heterojunction for boosted visible-light photocatalytic performance. J Chem Technol Biotechnol 96:1854–1863

[79] Guo F, Huang X, Chen Z, Cao L, Cheng X, Chen L, Shi W (2021) Construction of $Cu_3P\text{-}ZnSnO_3\text{-}g\text{-}C_3N_4$ p-n-n heterojunction with multiple built-in electric fields for effectively boosting visible-light photocatalytic degradation of broad-spectrum antibiotics. Sep Purif Technol 265:118477